Chinese Chemical Letters 37 (2026) 112448

Contents lists available at ScienceDirect

Chinese Chemical Letters

journal homepage: www.elsevier.com/locate/cclet

Discovery of novel and potent non-nucleoside reverse transcriptase inhibitors through structure-based drug design for HIV treatment

Yin-Xiang Zhang[a], Christophe Pannecouque[e], Erik De Clercq[e], Enzo Tramontano[f], Angela Corona[f], Laura Dettori[f], Phuong-Thao Tran[g], Xu-Dong Li[d], Shuo Su[c], Shuai Wang[a,b,*], Fen-Er Chen[a,*]

[a] Department of Chemistry, Engineering Center of Catalysis and Synthesis for Chiral Molecules, Shanghai Engineering Research Center of Industrial Asymmetric Catalysis of Chiral Drugs, State Key Laboratory of Green Chemical Synthesis and Conversion, Fudan University, Shanghai 200043, China
[b] State Key Laboratory of Natural and Biomimetic Drugs, Peking University, Beijing 100191, China
[c] Shanghai Institute of Infectious Disease and Biosecurity, School of Public Health, Fudan University, Shanghai 200032, China
[d] School of Data Science, Fudan University, Shanghai 200043, China
[e] Rega Institute for Medical Research, KU Leuven, Herestraat 49, Leuven B-3000, Belgium
[f] Dept Appl Sci Biosyst, University of Cagliari, Monserrato I-09042, Italy
[g] Department of Pharmaceutical Chemistry, Hanoi University of Pharmacy, 13-15 Le Thanh Tong, Cua Nam, Hanoi 10000, Vietnam

ARTICLE INFO

Article history:
Received 1 October 2025
Revised 21 January 2026
Accepted 22 January 2026
Available online 23 January 2026

Keywords:
HIV-1
NNRTIs
RT
Dihedral angle
Aqueous solubility

ABSTRACT

In this work, a series of novel non-nucleoside reverse transcriptase inhibitors featuring pyridine-difluoro/dimethylaniline fragment and 4-aminepiperidine moiety were synthesized based on structure-based design strategy. Among these, the dimethyl-substituted analogue **20m**, characterized by a larger dihedral angle, emerged as the most potent inhibitor against wild-type (WT) human immunodeficiency virus-1 (HIV-1) as well as multiple resistant strains. Compound **20m** exhibited remarkable antiviral activity with median effect concentration (EC_{50}) values of 0.003 μmol/L (WT), 0.011 μmol/L (L100I), 0.001 μmol/L (K103N), 0.006 μmol/L (Y181C), 0.108 μmol/L (Y188L), 0.008 μmol/L (E138K), 0.196 μmol/L (F227L+V106A), and 0.032 μmol/L (Y181C+K103N), consistently outperforming efavirenz (EFV). Notably, **20m** also demonstrated dramatically enhanced aqueous solubility, reaching >3954.5 μg/mL in phosphate buffer at pH 4.5 and >7380.6 μg/mL at pH 2.0, far exceeding that of etravirine (ETR). Collectively, these findings lay a robust foundation for the future optimization and development of next-generation non-nucleoside reverse transcriptase inhibitors (NNRTIs).

© 2026 Published by Elsevier B.V. on behalf of Chinese Chemical Society and Institute of Materia Medica, Chinese Academy of Medical Sciences.

Non-nucleoside reverse transcriptase inhibitors (NNRTIs) constitute an essential component of antiretroviral therapy (ART) for human immunodeficiency virus (HIV) treatment [1]. Etravirine (ETR) and rilpivirine (RPV), representative of diarylpyrimidine (DAPY) structures, are the second-generation NNRTIs approved by Food and Drug Administration (FDA) due to their favorable pharmacological profiles and excellent potency against diverse clinically relevant viral mutants (Fig. 1) [2–4]. The intrinsic structural flexibility of DAPY scaffolds enables compounds such as ETR and RPV to conformationally adapt to diverse allosteric binding pockets of both wild-type (WT) and mutant reverse transcriptase (RT) [5–7]. However, despite these advantages, both ETR and RPV display poor aqueous solubility and suboptimal pharmacokinetic (PK) properties inherent to their chemical structures. For example, the solubility of RPV is only about 20 ng/mL, while that of ETR is well below 1 μg/mL, rendering its oral bioavailability difficult to evaluate [8,9]. Furthermore, serious side effects like hepatotoxicity and hypersensitivity are continuously observed in patients receiving ETR and RPV regime, and the rapid emergency of drug resistance have greatly hampered their clinically applications [10,11].

In our previous work, we sought to overcome these deficiencies by modifying the cyanovinyl moiety of RPV (a known Michael acceptor) into a substituted cyano-naphthalene group (Fig. 1). The resulting compounds **1** and **2** exhibited potent antiviral activity against WT HIV-1, which was attributed to enhanced aromatic–aromatic interactions [12,13]. However, their efficacy against the RES056 (K103N+Y181C) strain was significantly diminished [14]. Furthermore, a simple replacement with a naphthalene ring was unlikely to improve solubility in theory. Recently, compound **3** with a bromo-substituted quinoline ring

* Corresponding authors.
E-mail addresses: shuaiwang@fudan.edu.cn (S. Wang), rfchen@fudan.edu.cn (F.-E. Chen).

https://doi.org/10.1016/j.cclet.2026.112448
1001-8417/© 2026 Published by Elsevier B.V. on behalf of Chinese Chemical Society and Institute of Materia Medica, Chinese Academy of Medical Sciences.

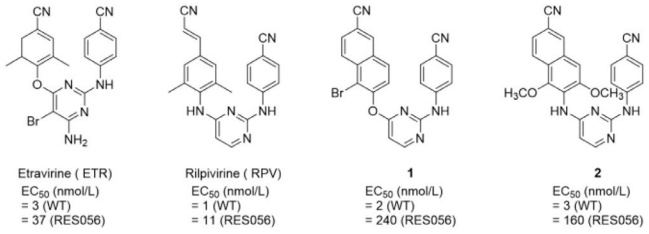


Fig. 1. The chemical structure of ETR, RPV and other DAYP compounds.

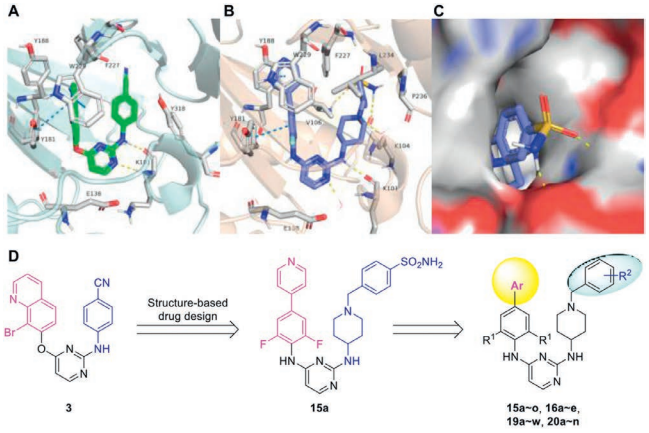
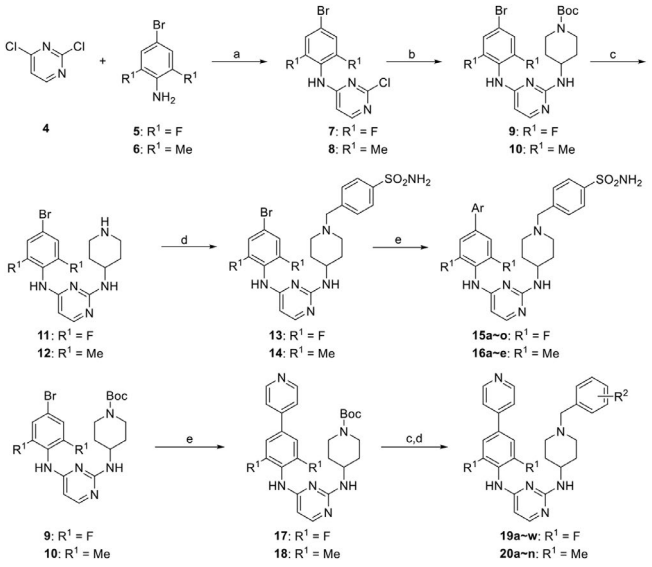


Fig. 2. (A) The docking mode of **3** in WT HIV-1 RT (PDB ID: 2ZD1). (B, C) the docking mode and surface pattern of **15a** in WT HIV-1 RT (PDB ID: 6C0N), respectively. (D) Rational design of target compounds.

on the left side was reported to exhibit significantly increased solubility of 26.02 μg/mL at pH 7.4 [15]. Although **3** exhibited potent activity against WT HIV-1 (median effect concentration (EC_{50}) = 1.8 nmol/L), it was largely inactive against a panel of mutant strains (Figs. 2A and D). By comparing the structure of **1**, **2**, **3**, ETR and RPV, these findings suggest that the key structural determinants governing the resistance profiles of ETR and RPV are likely located in the terminal nitrile (cyanovinyl) moiety and/or the dimethyl substituent, features that influence the dihedral angle between the central pyrimidine ring and the left-hand aromatic ring [16,17].

In this work, the dimethyl group on the left ring of the newly designed compounds was either retained or replaced with an isosteric difluoro moiety. Furthermore, inspired by the "necessary nitrogen atom" effect on solubility observed in compound **3**, a pyridine ring, a bioisostere of the cyano or cyanovinyl moiety, was introduced at the terminal position of the difluoro/dimethylaniline group (Fig. 2D) [18]. The electron-deficient pyridine ring promotes the formation of favorable face-to-face π–π stacking interactions, primarily driven by electrostatic complementarity, thereby enhancing binding affinity [19]. Fig. 2A illustrates this interaction between **3** and RT. In order to improve the resistance profile, the *para*-cyanophenyl ring on the right wing was replaced by privileged 4-aminopiperidine-linked benzyl scaffold, which was predicted to extend into the protein–solvent interface (Figs. 2B–D) [20,21]. Concurrently, the solubility was anticipated to be improved, as it disrupted the molecular symmetry characteristic of DAPY compounds and introduced several solubilizing motifs, such as the pyridine ring, an ionizable organic basic ring and the neutral hydrophilic group [22–26].

The synthetic routes of target compounds **15a**–**o**, **16a**–**e**, **19a**–**w** and **20a**–**n** were illustrated in Scheme 1. Using excess hydrochloric acid, starting material **4** was treated with **5** to harvest **7,** followed by a second nucleophilic substitution with excess 4-



Scheme 1. Reagents and conditions: (a) IPA/H_2O, HCl (conj, excess), r.t., 12–36 h; (b) 4-amino-1-Boc-piperidine (5.0 equiv.), neat, 120 °C, 12 h; (c) TFA, DCM, r.t., 4 h; (d) substituted benzyl bromide or chloride, DMF, K_2CO_3, r.t., 12 h; (e) aromatic boronic acid or esters, Pd(dppf)Cl_2, dioxane/H_2O, Cs_2CO_3, 110 °C, N_2, 12 h.

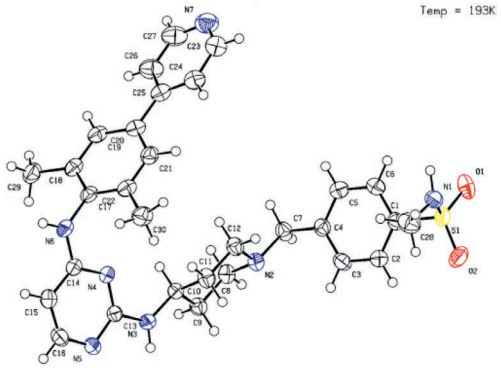


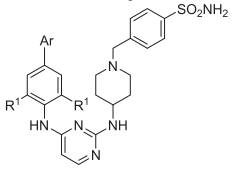
Fig. 3. The X-ray structure of compound **20b**.

boc-aminopiperidine to afford **9**. Then **11** was obtained by the deprotection of **9** and treated with 4-sulfonamide benzyl bromide to afford the common intermediate **13**, which was coupled with aromatic boronic acids or esters to afford target compounds **15a**–**o** [27,28]. The similar Suzuki–Miyaura coupling reaction was carried out on **9** to obtain **17**, followed by deprotection and continuous nucleophilic substitution to afford target compounds **19a**–**w**. A similar procedure was performed to give dimethyl derivatives **16a**–**e** and **20a**–**n**. To verify the regioselectivity of 2,4-dichlorinepyrimidine, the X-ray single crystal structure of **20b** was conducted and shown in Fig. 3.

All of the target compounds **15a**–**o**, **16a**–**e**, **19a**–**w** and **20a**–**n** were evaluated for their biological activity against WT HIV-1 (IIIB) and RES056 strains in MT-4 cell utilizing the MTT method [29]. Selected compounds were further screened for the antiviral activity against clinically frequently observed single/double mutant strains. Nevirapine (NPV), efavirenz (EFV) and ETR were selected as reference drugs. The values of EC_{50} (antiviral efficacy), concentration of cytotoxicity 50 % (CC_{50}) (cytotoxicity), selectivity index (SI, the ratio of CC_{50}/EC_{50}) and half maximal inhibitory concentration (IC_{50}) (enzymatic inhibitory potency) were organized in Tables 1–3.

First of all, we explored the effect of aromatic-difluoro/dimethylaniline fragment on their antiviral activity. Pleasingly,

Table 1
Antiviral activity of **15a–o** and **16a–e** against HIV-1 (IIIB) strains in MT-4 cells.



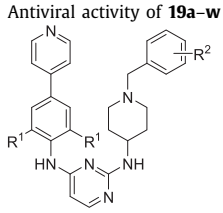
15a~o: R^1 = F
16a~e: R^1 = Me

Compd.	R^1	Ar	EC_{50} (WT) (μmol/L)	CC_{50} (μmol/L)	SI	Compd.	R^1	Ar	EC_{50} (WT) (μmol/L)	CC_{50} (μmol/L)	SI
15a	F		0.007 ± 0.003	3.3 ± 0.92	669	**15k**	F		0.073 ± 0.029	4.1 ± 0.78	56
15b	F		0.011 ± 0.004	4.1 ± 0.52	360	**15l**	F		0.021 ± 0.004	23.5 ± 2.82	832
15c	F		0.010 ± 0.008	8.2 ± 0.6	855	**15m**	F		0.007 ± 0.005	6.1 ± 1.43	1111
15d	F		0.010 ± 0.003	6.9 ± 0.91	668	**15n**	F		0.036 ± 0.013	22.8 ± 2.31	255
15e	F		0.012 ± 0.004	10.2 ± 3.03	350	**15o**	F		0.007 ± 0.001	2 ± 0.57	288
15f	F		0.026 ± 0.008	5.5 ± 0.98	311	**16a**	Me		0.008 ± 0.003	1.2 ± 0.42	0.24
15g	F		0.015 ± 0.004	4.1 ± 0.47	214	**16b**	Me		0.006 ± 0.001	4.2 ± 0.63	0.34
15h	F		0.044 ± 0.012	2.9 ± 0.72	183	**16c**	Me		0.007 ± 0.001	2.9 ± 0.92	3.94
15i	F		0.016 ± 0.007	5.7 ± 1.08	270	**16d**	Me		0.007 ± 0.002	4.2 ± 0.51	0.51
15j	F		0.050 ± 0.011	4.8 ± 0.9	98	**16e**	Me		0.007 ± 0.001	3.9 ± 0.46	0.26
NVP			0.188 ± 0.066	>15	>80	ETR			0.003 ± 0.001	>4.59	>1340
EFV			0.004 ± 0.002	>6.34	>1425						

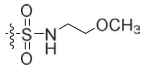
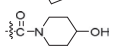
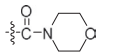
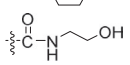
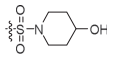
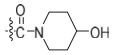
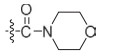
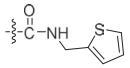
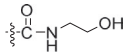
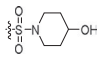
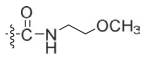
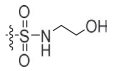
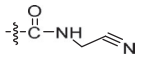
the newly synthesized compounds **15a–o** and **16a–e** showed moderate to potent inhibitory potency against WT HIV-1 (IIIB) (EC_{50} = 0.006–0.073 μmol/L) as depicted in Table 1. Based on the structural features and biological results, preliminary structure–activity relationship (SAR) was summarized. The antiviral activity was largely independent of the position of the pyridine nitrogen atom but was markedly governed by the substituents on the pyridine ring. For instance, the comparable potency of **15a** (EC_{50} = 0.007 μmol/L) and **15d** (EC_{50} = 0.010 μmol/L) resulted in a marginal delta pEC_{50} (ΔpEC_{50}) value of -0.15 ± 0.23 (Table S1 in Supporting information), indicating no significant difference in their activity. Typically, fluoro- and methoxy–substituents on the pyridine ring exhibited minimal positive effect on antiviral activity, whereas methyl, dimethylamino and trifluoromethyl groups led to significant reduction in potency. The methyl-substituted derivatives **15f** (EC_{50} = 0.026 μmol/L) and **15i** (EC_{50} = 0.050 μmol/L) showed 3.7- and 7.1-fold decrease in activity compared to **15a**, respectively. Interestingly, the pyrimidine analog **15L** also exhibited significantly reduced antiviral activity (EC_{50} = 0.020 μmol/L). Subsequent introduction of a methyl group at the 2-positition of the pyrimidine ring further diminished the potency (**15n**, EC_{50} = 0.036 μmol/L) albeit with lower cytotoxicity (CC_{50} = 22.8 μmol/L), conversely, methoxy substitution (**15m**) restored the potency (EC_{50} = 0.008 μmol/L). Besides, the comparable activity observed with the 4-cyanophenyl substitution (**15o**) to that of **15a** supported the feasibility of the pyridine ring replacement. Furthermore, the dimethyl analogs (**16a–e**) also exhibited potent activity against WT HIV-1 (EC_{50} = 0.006–0.007 μmol/L), which was substantially superior to NVP (EC_{50} = 0.188 μmol/L) and comparable to EFV (EC_{50} = 0.004 μmol/L) and ETR (EC_{50} = 0.003 μmol/L), as indicated by their ΔpEC_{50} values of 0.25 ± 0.29 and 0.37 ± 0.24 relative to **15a**. Based on these findings, the pyridine ring was identified as the preferred moiety attached to the left-hand difluoro/dimethylaniline ring.

In the second round of optimization, structurally diverse hydrogen donators/acceptors were installed on the right-hand phenyl scaffold to interrogate the protein/solvent interface and enable more favorable interactions. As depicted in Table 2, **19a–w** and **20a–n** maintained low nanomolar inhibitory activity against WT HIV-1 (IIIB) with EC_{50} values ranging from 0.002 μmol/L to 0.051 μmol/L. More specifically, the methyl-masking analog (**19a**) exhibited nearly identical antiviral activity to **15a**, while the slightly more lipophilic methylsulfonyl analog (**19b**) showed an approximately 2.3-fold increase in potency (EC_{50} = 0.003 μmol/L), with a ΔpEC_{50} value of 0.37 ± 0.19 supporting this enhancement (Table S2 in Supporting information). In this way, amide derivatives **19c–d** and ketone **19e** showed comparable antiviral potency relative to **15a**. Subsequently, more hydrophobic substituents (*e.g.*,

Table 2
Antiviral activity of **19a–w** and **20a–n** against HIV-1 (IIIB) strains in MT-4 cells.



19a~w: R^1 = F
20a~n: R^1 = Me

Compd.	R^1	R^2	EC_{50} (WT) (μmol/L)	CC_{50} (μmol/L)	SI	Compd.	R^1	R^2	EC_{50} (WT) (μmol/L)	CC_{50} (μmol/L)	SI
15a	F	4-SO_2NH_2	0.007 ± 0.003	3.3 ± 0.92	669	**19s**	F		0.003 ± 0.001	2.5 ± 0.99	724
19a	F	4-SO_2NHCH_3	0.006 ± 0.001	3.7 ± 0.96	604	**19t**	F		0.005 ± 0.001	3.8 ± 0.79	786
19b	F	4-SO_2CH_3	0.003 ± 0	4.7 ± 1.18	1584	**19u**	F		0.007 ± 0.001	3.8 ± 0.71	535
19c	F	4-$CONH_2$	0.004 ± 0.001	2.1 ± 0.28	544	**19v**	F		0.004 ± 0.001	3.7 ± 0.69	1081
19d	F	4-$CONHCH_3$	0.004 ± 0.001	8.7 ± 0.95	2156	**19w**	F		0.013 ± 0.005	22.2 ± 2.67	1695
19e	F	4-$COCH_3$	0.007 ± 0.003	4.6 ± 1.14	655	**20a**	Me	4-SO_2NH_2	0.005 ± 0.001	3.4 ± 0.75	760
19f	F	4-COOMe	0.051 ± 0.013	14.8 ± 9.28	288	**20b**	Me	4-SO_2NHCH_3	0.005 ± 0.001	1.3 ± 0.25	258
19g	F	4-F	0.012 ± 0.004	5 ± 0.64	418	**20c**	Me	4-$CONH_2$	0.006 ± 0.003	2.3 ± 1.12	408
19h	F	3-F	0.007 ± 0.002	5.2 ± 0.6	719	**20d**	Me	3-$CONH_2$	0.006 ± 0.002	3.2 ± 0.77	511
19i	F	2-F	0.012 ± 0.001	19.3 ± 8.34	1597	**20e**	Me	4-$CONHCH_3$	0.002 ± 0.001	3.1 ± 0.81	1962
19j	F	4-CN	0.012 ± 0.004	3.7 ± 0.92	320	**20f**	Me		0.006 ± 0.002	5.3 ± 12.42	923
19k	F	3-CN	0.009 ± 0.006	4.3 ± 0.91	488	**20g**	Me		0.005 ± 0.002	0.9 ± 0.27	180
19l	F	2-CN	0.007 ± 0.002	1.7 ± 0.23	488	**20h**	Me		0.005 ± 0.001	3.7 ± 0.57	763
19m	F	4-Cl	0.017 ± 0.005	4.9 ± 0.92	288	**20i**	Me		0.004 ± 0.001	3.1 ± 0.69	710
19n	F	4-CF_3	0.023 ± 0.008	4.1 ± 1.05	178	**20j**	Me		0.006 ± 0.001	1.1 ± 0.04	189
19o	F	4-Me	0.006 ± 0.002	3.3 ± 1.08	521	**20k**	Me		0.007 ± 0.001	1.5 ± 0.57	214
19p	F		0.008 ± 0.002	0.8 ± 0.15	98	**20l**	Me		0.006 ± 0.002	5.5 ± 0.38	971
19q	F		0.004 ± 0.001	0.9 ± 0.14	226	**20m**	Me		0.003 ± 0.001	3.3 ± 0.56	1215
19r	F		0.014 ± 0.005	4.3 ± 0.98	310	**20n**	Me		0.006 ± 0.001	2.6 ± 0.88	453
NVP			0.188 ± 0.066	>15	>80	ETR			0.003 ± 0.001	>4.59	>1340
EFV			0.004 ± 0.002	>6.34	>1425						

ester, fluoro, chloro, cyano, trifluoromethyl and methyl) were incorporated into the scaffold. Most of these modifications led to equivalent or marginally reduced activity, whereas ester (**19f**) and highly lipophilic trifluoromethyl groups (**19n**) caused the pronounced loss in potency against WT strain, reducing it by 7.3- and 3.3-fold compared with **15a**, respectively. To further investigate the effects of spatial occupancy and lipophilicity on biological activity, cyclic and bulkier substituents were also explored (**19p–q**, **19t–v**), which showed no significantly statistical differences in anti-WT activity relative to **15a**. More intriguingly, compound **19s**, bearing a methoxylethylsulfonamide terminus, exhibited superior anti-WT activity (EC_{50} = 0.003 μmol/L) compared to the hydroxyethylsulfonamide-terminated analog **19r** (EC_{50} = 0.014 μmol/L) and hydroxyethylamide-containing derivative **19w** (EC_{50} = 0.013 μmol/L), which featured a terminus of the same two-carbon chain length. The identical anti-WT activity trend was also observed in dimethyl series (**20a–n**). The order of antiviral potency for the short-chain hydrophilic groups was 4-$CONHCH_3$ (**20e**, EC_{50} = 0.002 μmol/L) >4-SO_2NH_2 ≈ 4-SO_2NHCH_3 ≈ 4-$CONH_2$ ≈ 3-$CONH_2$, with the activities of the latter four groups clustered in the range of 0.005–0.006 μmol/L. Besides, the analogs with cyclic and sterically demanding substituents (**20f–k**) exhibited excellent anti-HIV-1 (IIIB) activity, with no significant difference in potency observed among them. Regarding to two-carbon chain end, **20m** (EC_{50} = 0.003 μmol/L) with methoxylethylamide appendage was more potent than analogs **20L** and **20n** (EC_{50} = 0.006 μmol/L).

Subsequently, compounds **15a–b**, **16a–b**, **16d**, **19b–c**, **19s**, **19v**, **20a–b**, **20e** and **20m** with high potency against WT HIV-1 (IIIB) were further selected to assess their efficacy against clinically prevalent single mutant strains (L100I, K103N, Y181C, Y188L and E138K) and double mutant strains (F227L+V106A and RES056) as well as WT HIV-1 RT. As depicted in Table 3, it was noticeable that all tested compounds exhibited superior potency against the

Table 3
Inhibitory activity of representative compounds toward seven mutant strains and HIV-1 RT.

Compd.	EC_{50} (μmol/L)							IC_{50} (μmol/L)
	L100I	K103N	Y181C	Y188L	E138K	F227L+V106A	RES056	
15a	0.156 ± 0.041	0.041 ± 0.016	0.127 ± 0.057	≥0.943	0.048 ± 0.018	≥5.892	≥5.892	0.100 ± 0.018
15b	0.350 ± 0.053	0.063 ± 0.013	0.072 ± 0.012	>4.12	0.098 ± 0.067	>4.12	>4.12	0.091 ± 0.029
16a	0.054 ± 0.007	0.008 ± 0	0.042 ± 0.003	0.923 ± 0.032	0.055 ± 0.012	>0.264 ± 0	0.248 ± 0.064	0.182 ± 0.009
16b	0.061 ± 0.013	0.008 ± 0.002	0.036 ± 0.003	0.245 ± 0.045	0.053 ± 0.006	0.355 ± 0.097	0.247 ± 0.05	0.148 ± 0.001
16d	0.065 ± 0.011	0.006 ± 0.002	0.034 ± 0.012	0.286 ± 0.07	0.034 ± 0.013	0.234 ± 0.124	0.209 ± 0.097	0.199 ± 0.019
19b	0.094 ± 0.008	0.008 ± 0.001	0.059 ± 0.02	>1.344	0.017 ± 0.005	>0.926	>4.675	0.091 ± 0.031
19c	0.004 ± 0.001	0.004 ± 0.001	0.004 ± 0.001	>2.139	0.024 ± 0.005	>2.139	>2.139	0.074 ± 0.008
19d	0.208 ± 0.158	0.021 ± 0.012	0.057 ± 0.019	1.185 ± 0.118	0.018 ± 0.002	>8.653	>8.653	0.135 ± 0.025
19s	0.194 ± 0.25	0.006 ± 0.002	0.025 ± 0.008	0.722 ± 0.208	0.015 ± 0.002	>3.836	>3.836	0.109 ± 0.050
19v	0.36 ± 0.136	0.056 ± 0.01	0.108 ± 0.034	>3.74	0.042 ± 0.003	7.295 ± 1.574	3.106 ± 0.361	0.178 ± 0.052
20a	0.024 ± 0.014	0.004 ± 0.001	0.012 ± 0.005	0.205 ± 0.064	0.017 ± 0.007	0.383 ± 0.07	0.12 ± 0.016	0.087 ± 0.043
20b	0.017 ± 0.006	0.004 ± 0.001	0.016 ± 0.008	0.213 ± 0.022	0.029 ± 0.008	0.690 ± 0.476	0.093 ± 0.011	0.132 ± 0.009
20e	0.026 ± 0.008	0.003 ± 0.001	0.010 ± 0.001	0.365 ± 0.055	0.015 ± 0.001	0.550 ± 0.343	0.176 ± 0.046	0.164 ± 0.061
20m	0.011 ± 0.004	0.001 ± 0.001	0.006 ± 0.001	0.108 ± 0.047	0.008 ± 0.003	0.196 ± 0.084	0.032 ± 0.011	0.209 ± 0.002
NVP	1.79 ± 1.426	5.872 ± 2.777	9.019 ± 2.619	>15	0.141 ± 0.039	>15	>15	0.976 ± 0.338
EFV	0.030 ± 0.015	0.084 ± 0.033	0.008 ± 0.003	0.303 ± 0.127	0.008 ± 0.003	0.267 ± 0.368	0.327 ± 0.194	0.011 ± 0.025
ETR	0.007 ± 0.005	0.003 ± 0.001	0.016 ± 0.005	0.02 ± 0.008	0.009 ± 0.004	0.015 ± 0.013	0.041 ± 0.026	0.030 ± 0.005
3	0.340 ± 0.072	0.069 ± 0.014	0.220 ± 0.096	7.19 ± 4.64	0.045 ± 0.022	2.53 ± 1.06	11.57 ± 9.062	0.011 ± 0.001

L100I, K103N, Y181C, and E138K mutant strains. However, against the Y188L strain and the two double mutants (F227L+V106A and RES056), a clear divergence was observed between the difluoro and dimethyl series (**15a**–**b** *vs*. **16a**–**b**, **16d**; **19b**–**c**, **19s**, **19v** *vs*. **20a**–**b**, **20e**, **20m**) that the difluoro analogs were more sensitive and even substantially lost their activities, whereas the dimethyl analogs largely maintained their potency. Among them, **20m** demonstrated to be the most potent inhibitors, with EC_{50} values of 0.011 μmol/L (L100I), 0.001 μmol/L (K103N), 0.006 μmol/L (Y181C), 0.108 μmol/L (Y188L), 0.008 μmol/L (E138K), 0.196 μmol/L (F227L+V106A), 0.032 μmol/L (RES056), outperforming **3** and EFV, slightly inferior to ETR. Concurrently, to confirm the binding target of these compounds, their inhibitory activity against the recombinant WT HIV-1 RT were also evaluated with IC_{50} values of 0.074–0.209 μmol/L, being superior to NVP (IC_{50} = 0.976 μmol/L). Among them, **15b** (IC_{50} = 0.091 μmol/L), **19b** (IC_{50} = 0.091 μmol/L), **19c** (IC_{50} = 0.074 μmol/L) and **20a** (IC_{50} = 0.087 μmol/L) were identified as the four most effective inhibitors with robust RT inhibitory potency. Notably, these compounds exhibited marked disparity in potency, with cellular-level inhibition substantially exceeding that at the enzyme level *in vitro*. This observation may be attributed to multiply factors, such as cellular accumulation yielding elevated local concentration at the target site, intracellular metabolic activation, prolonged target residence time and potential multi-target synergistic effects. Collectively, the HIV-1 RT inhibition assay demonstrated potent binding of these novel derivatives to RT, indicating that they could be regarded as HIV-1 NNRTIs.

In order to explain the discrepancy of antiviral activity, molecular docking was employed to predict the binding modes of **20m** or difluoro analogs with WT HIV-1 RT and mutants. As depicted in Fig. 4A, **20m** binds to the active binding pocket of WT HIV-1 RT in a "U-shaped" conformation, similar to classic NNRTIs. The left-hand pyridine-dimethylaniline fragment was capable of fitting well into the hydrophobic tunnel constituted by residues Y181, Y183, Y188, F227 and highly conserved W229. Especially for Y188 residue, the electron-deficient pyridine ring is conducive to forming preferable face-to-face π-π stacking, an interaction more driven by electrostatic complementarity in nature than aromatic hydrophobic effects, thereby contributing to improvement in binding affinity. Besides, an important hydrogen bond between **20m** and K101 is retained, consistent with binding of other DAPYs. Additionally, water-mediated hydrogen bonds are also observed at the position of N atom of central pyrimidine or the N atom of piperidine ring. At the protein/solvent interface, the terminal oxygen atom of **20m** engages in another hydrogen bond with residue V106. Collectively, Given the multitude of critical interactions observed, it is rational that **20m** exhibits high potency against WT HIV-1 RT.

However, with respect to Y188L mutant, the robust π-π stacking is disrupted and a weaker aromatic hydrophobic interaction between Y181 and dimethyl-phenyl ring enforces to strengthen as a compensation, which partially compromised the antiviral activity of **20m** against the Y188L strain (Fig. 4B). More interestingly, the dihedral angle between dimethylaniline ring and central pyrimidine ring, that is C(14)-N(6)-C(17)-C(22) of **20m**, varies greatly when **20m** adapts itself to WT or Y188L RT (Figs. 4C and D). when bound to WT HIV-1 RT, **20m** adopts a dihedral angle of 74.5°, whereas the angle shifts to 86.4° in the Y188L RT complex. The dihedral angle of **20m** in the WT complex is closer to that of observed in the X-ray structure of **20b** (−70.8°, Fig. 3), which means that the conformation of **20m** in the WT complex likely resembles its dominant solution conformation and requires minimal torsional or rotational adjustment to adapt to the binding pocket. In contrast, there will be more entropy loss of **20m** in the Y188L RT complex. As for RES056 mutant, **20m** exhibited robust inhibitory potency which can be evidenced by Fig. 4E. Despite Y181C and K103N double mutations, the pyridine-dimethylaniline fragment enhances interactions with residue Y188 and the conserved W229. Furthermore, an additional hydrogen bond between the terminal amide NH and the backbone oxygen atom of K104 is observed, further contributing to the binding affinity. In the case of the F227L+V106A mutant, however, the scenario differs significantly. The π-π stacking is markedly weakened due to a substantial shift of the entire binding pocket (Fig. 4F). Structural superposition of the **20m**/F227L+V106A and RES056 complexes reveals notable displacements: the centroid of residue Y183 is shifted by 6.3 Å, and that of Y188 by 2.8 Å (Fig. 4G). Furthermore, residue L227 is positioned further away compared to F227. Although the hydrogen bond interacted with A106 is retained, the critical aromatic interactions are substantially lost, which mainly accounts for the weakened activity against this mutant. Moreover, the predicted dihedral angle of **20m** counts again, that is 54.7° in F227L+V106A RT complex, shift 19.8° away from that in WT complex. Besides, other docking dihedral angles are 78.9° (L100I), 64.6° (K103N), 81.1° (Y181C), 68.1° (E138K) and 68.4° (RES056).

Another phenomenon is that difluoro derivatives are mainly sensitive to the mutation of HIV-1 RT, which can be attributed to

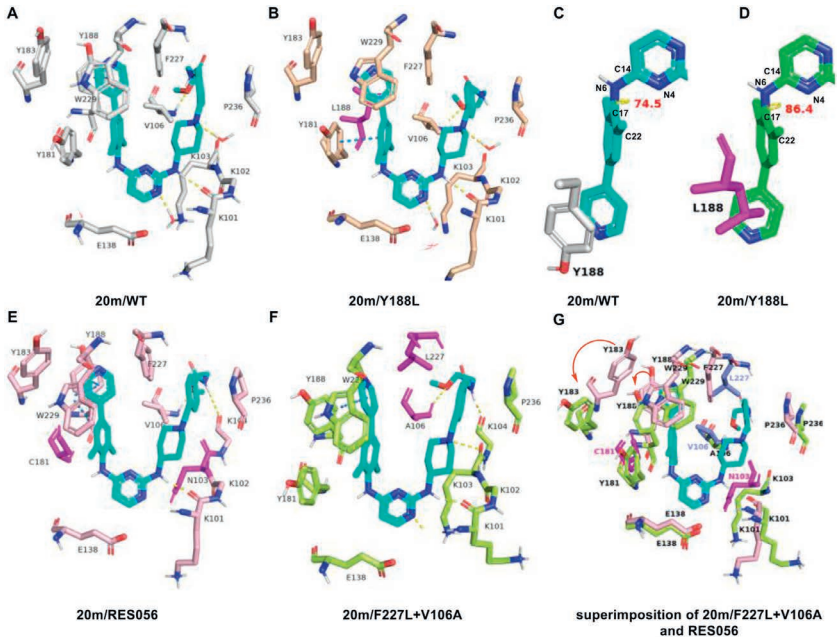


Fig. 4. The docking pattern of **20m** with WT HIV-1 RT and mutants. (A) WT (PDB code: 6C0N, in gray). (B) Y188L (PDB code: 6C0N, in wheat). (C, D) Different dihedral configurations of C(14)-N(6)-C(17)-C(22) of **20m** (in cyan or green) in WT and Y188L, respectively. (E) RES056 (PDB code: 6C0R, in light pink). (F) F227L+V106A (PDB code: 6DUF, in limon). (G) Superimposition of **20m** with F227L+V106A and RES056. Mutated residues are depicted as magentas sticks (or slate sticks). Hydrogen bonds are showed as yellow dashed lines and π-π stacking contacts are illustrated as marine dashed lines.

their dihedral configurations. The preferred conformations of **20b** (Fig. 3) or **20m** (Fig. 4D) support that the dimethylaniline moiety is closely perpendicular to the central pyrimidine ring (−70.8° and 74.5°) and the lone pairs on the N^4H and N^6 atoms favor a *trans*-figuration. Thus, a steric clash is likely to happen when the methyl substitute approach to the N^4 atom due to lone pair repulsion. In contrast, the favorable interaction of a $N \rightarrow F$ ($n_N \rightarrow \sigma^*F$) will be formed that induces the fluorine atom more closely to pyrimidine ring resulting to smaller dihedral angle. As expected, the docking dihedral angle of **15a** in WT complex is 62° convinces this hypothesis. Consequently, the relatively rigid structures of difluoro analogs reflect reduced flexibility when adapted to diverse binding pockets of mutants, necessitating the overcoming of greater rotational energy barriers and leading to inferior anti-resistant activity.

To further elucidate the potency, **20m** complexed with the RES056 are subjected to molecular dynamics (MD) simulation. From Fig. S1 (Supporting information), it can be seen that their root-mean-square deviation (RMSD) values were kept below 3.5 Å, indicating the strong binding affinity and low probability of dissociation. Four primary types of interactions exist: ionic interactions, hydrogen bonds, hydrophobic contacts, and water-bridged bonds. The analysis demonstrates that residue K101 form a very significant and stable hydrogen bond with **20m** for 97 % of the simulation time during the trajectory process. Besides, the three critical water-bridge/hydrogen bonds formed by residues K101, V106, and Q222. The binding is further stabilized by significant π-π stacking interactions between the left-wing heterobiaryl fragment of **20m** and residues Y188, F227, and W229. The mean dihedral angle for **20m** is 68.44° ± 9.63°, which is consistent with the value measured in the molecular docking analysis. Collectively, the protein-ligand contacts effectively account for the potent potency of **20m** against RES056. Eventually, the aqueous solubility of **20m** was also assessed in different phosphate buffer solutions (pH 7.4, 4.5 and 2.0) in Table 4. Gratifyingly, the aqueous solubility of **20m** was markedly enhanced, particularly in acidic buffers, reaching >3954.5 μg/mL at pH 4.5 and >7380.6 μg/mL at pH 2.0, far surpassing the solubility of both compound **3** and ETR.

Table 4
The aqueous solubility of **20m**.

Compd.	Solubility (μg/mL)		
	pH 2.0	pH 4.5	pH 7.4
20m	>7380.6	>3954.5	0.32
3	28.49	N/A	26.02
ETR	127	N/A	≪1

In conclusion, we have synthesized a series of novel compounds incorporating a substituted pyridine–difluoro/dimethylaniline fragment and a 4-aminopiperidine moiety by employing structure-based drug design strategy. The electron-deficient pyridine ring enhanced π–π stacking interactions, thereby improving binding affinity. At the protein–solvent interface, hydrophilic substitutions proved more favorable than lipophilic groups. SAR analysis further revealed that dimethyl analogs displayed stronger antiviral activity than their difluoro counterparts, particularly against the Y188L mutant and the double mutations (F227L+V106A, RES056). This difference in activity was likely associated with variations in the dihedral angle between the pyridine–difluoro/dimethylaniline fragment and the adjacent moiety. The dimethyl analog adopted a larger dihedral angle, whereas the difluoro analog were predicted to have a smaller one and conferred a more rigid conformation, reducing flexibility to compromise its ability to adapt to diverse mutant binding pockets and thus leading to a significant decrease in potency. The dimethyl derivative **20m** demonstrated the efficacy of this strategy, exhibiting not only excellent antiviral potency against WT HIV-1 and seven mutant strains (EC_{50} = 0.003–0.196 μmol/L) but also significantly improve solubility profile (S > 3954.5 μg/mL at pH 4.5; S > 7380.6 μg/mL at pH 2.0), dramatically higher than that of **3** and ETR.

Declaration of competing interest

The authors declare that they have no known competing financial interests or personal relationships that could have appeared to influence the work reported in this paper.

CRediT authorship contribution statement

Yin-Xiang Zhang: Writing – original draft, Formal analysis, Data curation. **Christophe Pannecouque:** Writing – original draft, Resources, Formal analysis, Data curation. **Erik De Clercq:** Writing – review & editing, Conceptualization. **Enzo Tramontano:** Writing – review & editing, Resources. **Angela Corona:** Writing – review & editing, Resources. **Laura Dettori:** Writing – original draft, Resources. **Phuong-Thao Tran:** Writing – review & editing, Project administration. **Xu-Dong Li:** Writing – review & editing, Writing – original draft, Formal analysis, Data curation. **Shuo Su:** Writing – review & editing, Formal analysis, Data curation. **Shuai Wang:** Writing – review & editing, Supervision, Project administration, Funding acquisition, Data curation, Conceptualization. **Fen-Er Chen:** Writing – review & editing, Supervision, Resources, Project administration, Conceptualization.

Acknowledgments

This work was financially supported by the National Natural Science Foundation of China (Nos. 82574236 and 82304297), Shanghai Pujiang Programme (No. 23PJD005), the State Key Laboratory of Natural and Biomimetic Drugs (No. K202408), and Shanghai Pilot Program for Basic Research-Fudan University 21TQ1400100 (No. 25TQ011).

Supplementary materials

Supplementary material associated with this article can be found, in the online version, at doi:10.1016/j.cclet.2026.112448.

References

[1] Q. Hao, X. Ling, C. Pannecouque, et al., Chin. Chem. Lett. 34 (2023) 107663.
[2] K. Zhang, Y.J. Zhang, M. Li, et al., Med. Res. Rev. 45 (2024) 426–483.
[3] L.M. Zhao, C. Pannecouque, E. De Clercq, et al., Chin. Chem. Lett. 34 (2023) 108261.
[4] S. Du, X. Liu, X. Hu, et al., Chin. Chem. Lett. 36 (2025) 110378.
[5] V. Poongavanam, V. Namasivayam, M. Vanangamudi, et al., WIREs Comput. Mol. Sci. 8 (2017) e1328.
[6] E.B. Lansdon, K.M. Brendza, M. Hung, et al., J. Med. Chem. 53 (2010) 4295–4299.
[7] K. Das, P.J. Lewi, S.H. Hughes, et al., Prog. Biophys. Mol. Biol. 88 (2005) 209–231.
[8] Y. Sang, S. Han, C. Pannecouque, et al., J. Med. Chem. 62 (2019) 11430–11436.
[9] X.M. Chen, Q.Q. Hao, C. Pannecouque, et al., Acta Pharm. Sin. B 15 (2025) 4115–4136.
[10] Z. Wang, W.A. Zalloum, W. Wang, et al., J. Med. Chem. 64 (2021) 13658–13675.
[11] Z. Wang, P.P. Sharma, B. Rathi, et al., J. Med. Chem. 66 (2023) 8643–8665.
[12] Y.H. Liang, X.Q. Feng, Z.S. Zeng, et al., ChemMedChem 4 (2009) 1537–1545.
[13] X.Q. Feng, Y.H. Liang, Z.S. Zeng, et al., ChemMedChem 4 (2009) 219–224.
[14] Y.H. Liang, Q.Q. He, Z.S. Zeng, et al., Biorg. Med. Chem. 18 (2010) 4601–4605.
[15] R.L. Zhou, C. Yu, C. Pannecouque, et al., Bioorg. Chem. 140 (2023) 106821.
[16] J. Che, X. Dai, J. Gao, et al., J. Med. Chem. 64 (2021) 12163–12180.
[17] J. Chandrasekhar, R. Dick, J. Van Veldhuizen, et al., J. Med. Chem. 61 (2018) 6858–6868.
[18] L.D. Pennington, D.T. Moustakas, J. Med. Chem. 60 (2017) 3552–3579.
[19] M.A.M. Subbaiah, N.A. Meanwell, J. Med. Chem. 64 (2021) 14046–14128.
[20] K. Zhang, L. Zhao, T. Xing, et al., Chin. Chem. Lett. 37 (2026) 111283.
[21] B. Meng, Z. Zhuo, H. Yu, et al., Chin. Chem. Lett. 35 (2024) 100827.
[22] M. Ishikawa, Y. Hashimoto, J. Med. Chem. 54 (2011) 1539–1554.
[23] F. Lovering, J. Bikker, C. Humblet, J. Med. Chem. 52 (2009) 6752–6756.
[24] F. Lovering, MedChemComm 4 (2013) 515–519.
[25] X. Lin, H. Shi, W. Zhang, et al., J. Med. Chem. 62 (2019) 10352–10361.
[26] Y. Wu, L. Zhang, Z. Sun, et al., J. Med. Chem. 66 (2023) 8545–8563.
[27] M. Yang, Y. Liu, X. Qi, et al., Green Syn. Catal. 5 (2024) 211–269.
[28] B. Qiu, Y.F. Shi, X.D. An, et al., Green Syn. Catal. 6 (2025) 110–113.
[29] C. Pannecouque, D. Daelemans, E. De Clercq, Nat. Protoc. 3 (2008) 427–434.